Study of Supramolecular Side-Chain Copolymers Containing Light-Emitting H-Acceptors and Electron-Transporting Dendritic H-Donors

Po-Jen Yang, Chung-Wen Wu, Duryodhan Sahu, and Hong-Cheu Lin*

Department of Materials Science and Engineering, National Chiao Tung University, Hsinchu, Taiwan, ROC

Received May 3, 2008; Revised Manuscript Received October 27, 2008

ABSTRACT: A novel light-emitting hydrogen-bonded (H-) acceptor **PBB (M1)** containing three conjugated aromatic rings, including one pyridyl terminus and two lateral methoxyl groups (on the middle ring), was successfully synthesized via Horner−Wadsworth−Emmons (HWE) olefination and Sonogashira coupling reaction. Moreover, different molar ratios of light-emitting H-acceptor monomer **PBB (M1)** and hole-transporting monomer **CAZ (M2)** bearing a carbazole unit were copolymerized through free radical polymerization to obtain light-emitting and hole-transporting H-acceptor copolymers **(P1−P5)**. H-acceptor copolymers **P3** and **P4** were complexed with different generations of dendritic H-donors **(G1COOH−G3COOH)** bearing 1,3,4-oxadiazole (**OXD**) dendrons and terminal benzoic acids via H-bonded self-assembly to form supramolecular side-chain copolymers (i.e., H-bonded dendritic complexes). In contrast to H-acceptor homopolymer **P1 (HPBB)**, H-acceptor copolymers **P2−P4** incorporated with carbazole (**CAZ**) moieties effectively enhance the glass transition temperatures (T_gs) and minimize the interchain interations of the light-emitting H-acceptor units, and similar effects occur in their H-bonded dendritic complexes. In addition, red shifts of photoluminescence (PL) emissions in H-bonded dendritic complexes can be tuned up to 61 nm. Furthermore, H-bonded dendritic complexes excited at 305 nm of **OXD** absorption can create a stronger fluorescence than that excited at 397 nm of **PBB** absorption, indicating that the intensity of the sensitized emission of **PBB** (by energy transfer from **OXD** absorption at 305 nm) is even stronger than that of a direct emission of **PBB** (by merely **PBB** absorption at 397 nm). The **OXD** dendritic wedges in H-bonded dendritic complexes can lower the LUMO energy levels and provide a better electron injection property. H-acceptor polymer **P4** and its H-bonded dendritic complexes showed electroluminescence (EL) emissions in the range of 464−519 nm from blue to green. In addition, a PLED device containing H-bonded dendritic complex **P4/G1COOH** showed an EL emission of 519 nm under a turn-on voltage of 6.5 V, with a maximum luminance of 408 cd/m^2 at 18 V and a luminance efficiency of 0.39 cd/A at 100 mA/cm^2, respectively.

Introduction

In recent years, polymeric materials based on spontaneous formation of supramolecular architectures by self-assembly of various organic molecular components have attracted great attention in areas ranging from chemistry to materials science.[1,2] Simple association of two complementary compounds through specific noncovalent interactions, such as hydrogen-bonded (H-bonded),[3−8] ionic,[9,10] and metal-coordinative[11−15] interactions between molecular components, can give rise to unique properties and phase structures, which are not possessed by the individual components. Intensive researches have been directed toward functional supramolecular systems to control the dimensionality and shape of self-assembled structures through molecular design, but it remains a challenge driven by a wide variety of potential applications in the fields of catalyzes, microelectronics, nonlinear optics, sensors, and display technologies.

Since the first polymeric light-emitting diode (PLED) based on poly(*p*-phenylenevinylene) (PPV) was reported by Burroughes et al.,[16] various kinds of conjugated main-chain and side-chain polymers have been developed for electroluminescent (EL) devices.[17−20] Future applications of PLEDs to full-color and large-area flat panel displays become possible due to their high luminescence efficiency, low cost, high flexibility, and easy fabrication of spin-coating technique.[21] However, the most important problem with the π-conjugated systems is their tendency to form aggregates/excimers via $\pi-\pi$ interactions in the solid state, which will lead to red shifts or low-energy band gaps of emission spectra, self-quenching of excitons, and reduction of fluorescence quantum efficiencies. To overcome this problem, one of the approaches is to introduce dendritic architectures into the π-conjugated systems so as to prevent close chains from packing and thus to increase the polymer luminescent efficiency and reduce the tendency of aggregation. For instance, Fréchet-type poly(aryl ether) dendrons attached to fluorene units were reported by Carter et al.[22] to demonstrate the shielding effect by attaching dendritic side chains to the conjugated polyfluorene backbones, which improved the luminescence properties of these materials due to the reduction of both aggregates/excimers in solution and solid states. Müllen et al.[23] prepared polyfluorene-based conjugated polymers with bulky polyphenylene dendritic substituents at C-9 position, which suppressed the formation of aggregates with long wavelength emissions, and thus a pure blue emission was acquired. More recently, a number of dendrimers have been reported for a wide variety of applications in such EL device[24−34] and photovoltaic (PV) cell[35,36] materials.

In our previous work,[37] H-donor dendrimers with a benzoic acid terminus were singly/doubly H-bonded to mono/bis-pyridyl H-acceptor emitters to form several series of novel supramolecular dendrimers, whose emission colors could be easily adjusted by their non-light-emitting H-donors. Moreover, the higher generation of dendritic sizes could afford stronger site-isolation and dendron-dilution effects, so better energy transfer along with higher fluorescence quantum efficiencies were achieved.

In the present study, our strategy is to extend the π-conjugated system from H-acceptor emitters of small molecules to light-emitting H-acceptor polymers. According to Scheme 1, a series

* Corresponding author: Tel 8863-5712121ext 55305; Fax 8863-5724727; e-mail linhc@mail.nctu.edu.tw.

10.1021/ma801005c CCC: $40.75
Published on Web 11/18/2008

Scheme 1. Synthetic Routes of H-Acceptor Monomer and Polymers (P1−P5)[a]

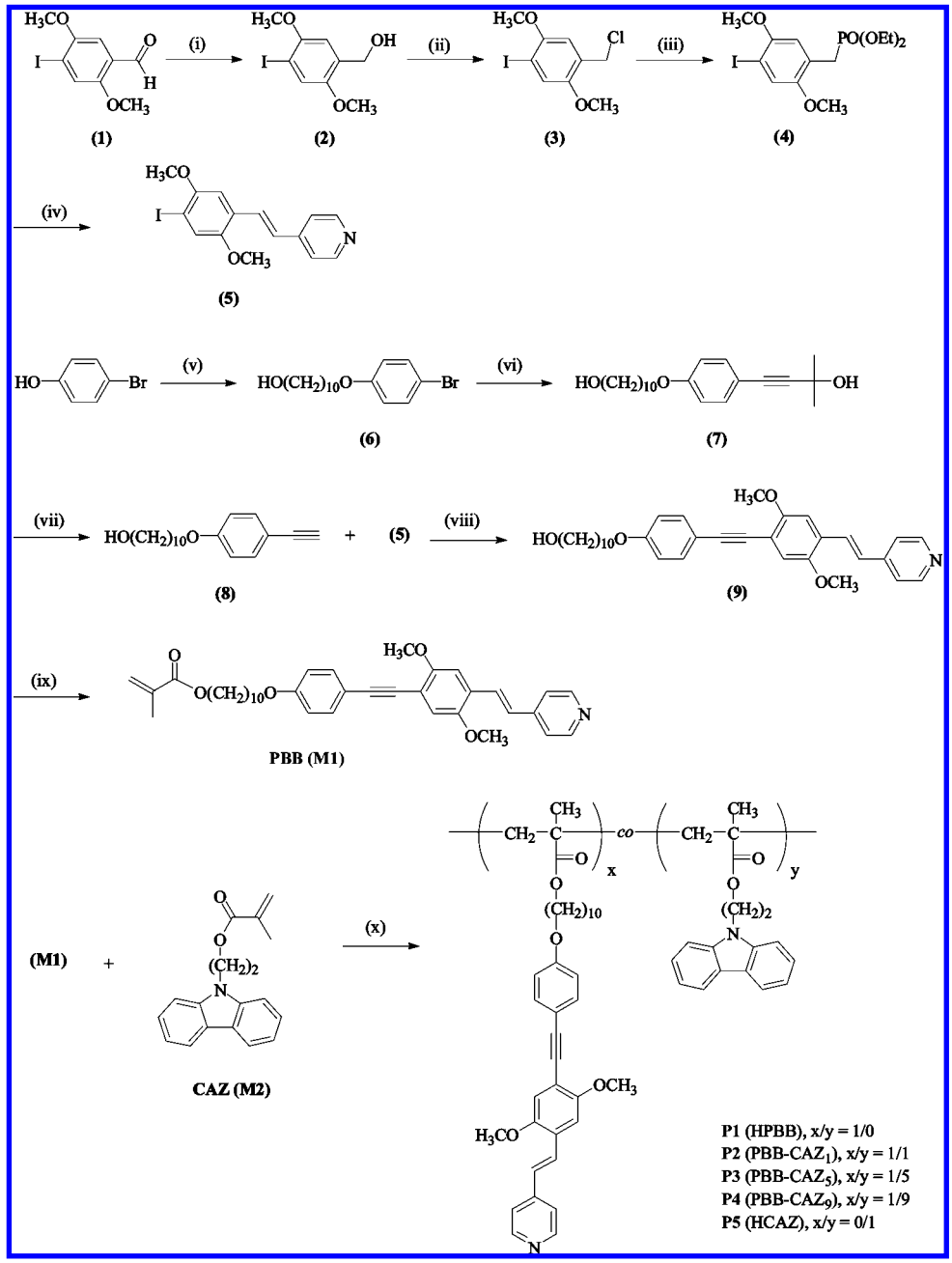

[a] Reagents and conditions: (i) $NaBH_4$, MeOH/THF, room temperature, 1 h; (ii) concentrated HCl, dioxane, reflux, 10 h; (iii) $P(OEt)_3$, reflux, 12 h; (iv) pyridine-4-carboxaldehyde, *t*-BuOK, THF, room temperature, 12 h; (v) 10-bromodecanol, K_2CO_3, KI, acetone, reflux, 48 h; (vi) 2-methyl-3-butyn-2-ol, $Pd(PPh_3)_2Cl_2$, CuI, PPh_3, Et_3N, 70 °C, 12 h; (vii) KOH, dioxane, reflux, 3 h; (viii) $Pd(PPh_3)_2Cl_2$, CuI, PPh_3, Et_3N/THF, 50 °C, overnight; (ix) vinyl methacrylate, 1,3-dichloro-1,1,3,3-tetrabutyldistannoxane, 2,6-di-*tert*-butyl-4-methylphenol, THF, 50 °C, 48 h; (x) AIBN, THF, 60 °C, 24 h.

of novel homopolymeric and random-copolymeric H-acceptor emitters containing carbazole moieties (to increase T_g values and hole-transporting properties of PLEDs) and three-conjugated aromatic rings, including one pendent pyridyl terminus (as the H-acceptor site) and two lateral methoxyl groups on the middle rings (to increase solubility after polymerization), were successfully synthesized. By incorporating with different generations of **OXD** dendritic H-donors bearing benzoic acids (see Figure 1), the supramolecular side-chain copolymers (i.e., H-bonded dendritic complexes) were consecutively constructed as shown in Figure 2. Hopefully, supramolecular dendrimers bearing light-emitting H-acceptor polymers (in comparison with small molecular emitters) will have a better film-forming property by the spin-coating process, which may eventually be more useful in PLED device applications. Accordingly, H-bonded effects on the thermal, photophysical, and photo/electroluminescent properties of these supramolecules in the solid state will be illustrated.

Experimental Section

Measurements and Characterization. ^1H NMR spectra were recorded on a Varian Unity 300 MHz spectrometer using $CDCl_3$ and DMSO-d_6 as solvents. Elemental analyses were performed on a HERAEUS CHN-OS RAPID elemental analyzer. High-resolution electron impact mass data were obtained on a Finnigan-MAT-95XL. Phase transition temperatures were determined by differential scanning calorimetry (DSC, model: Perkin-Elmer Diamond) under N_2 with a heating and cooling rate of 10 °C/min and polarizing

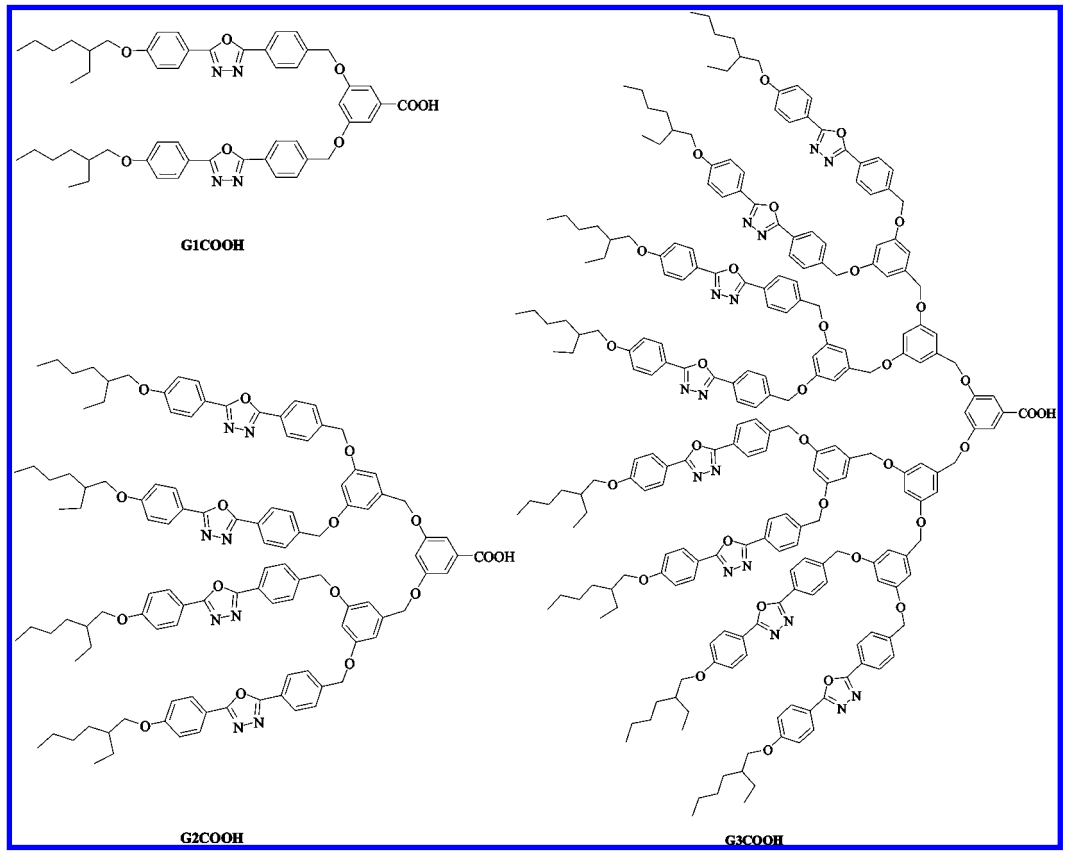

Figure 1. Different generations of dendritic H-donors (**G1COOH**−**G3COOH**) used in H-bonded side-chain dendritic complexes.

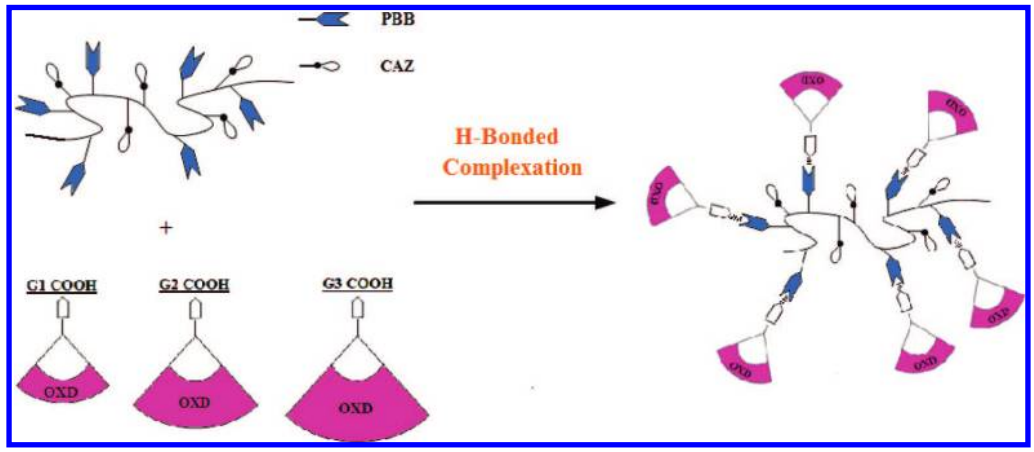

Figure 2. Schematic representation of H-acceptor copolymers and H-bonded side-chain dendritic complexes bearing different generations of dendritic H-donors (**G1COOH**−**G3COOH**).

optical microscope (POM, model: Leica DMLP) equipped with a hot stage. Thermogravimetric analyses (TGA) were carried out on a TA Instruments Q500 thermogravimetric analyzer at a heating rate of 20 °C/min under nitrogen. Gel permeation chromatography (GPC) analyses were conducted on a Waters 1515 separation module using polystyrene as a standard and THF as an eluant. Fourier transform infrared (FTIR) spectra of samples (dispersed in KBr disks) were recorded on a Perkin-Elmer Spectrum 100 Series. Synchrotron powder X-ray diffraction (XRD) measurements were performed at the beamline BL17A of the National Synchrotron Radiation Research Center (NSRRC), Taiwan (for details of the XRD installation, see Supporting Information). UV−vis absorption spectra were recorded on a HP G1103A spectrophotometer, and photoluminescence (PL) spectra were obtained on a Hitachi F-4500 spectrophotometer in dilute THF solutions (10^{-6} M). The PL quantum yields (Φ_{PL}) of polymers were measured with 9,10-diphenylanthracene as a reference (in cyclohexane, $\Phi_{PL} = 0.9$).[38] Thin films in UV−vis and PL measurements were prepared by spin-coating of THF solutions (with a concentration of 10 mg/mL) at 3000 rpm on a quartz substrate. Cyclic voltammetry (CV) measurements were performed at a scanning rate of 100 mV/s in a solution of 0.1 M tetrabutylammonium hexafluorophosphate (Bu_4NPF_6) dissolved in acetonitrile at room temperature using an Autolab PGSTAT30 potentiostat/galvanostat with a standard three-electrode electrochemical cell. A platinum disk working electrode, a Pt wire counter electrode, and an Ag/AgCl reference electrode were used. The sample films were coated on the surface of a platinum disk by the solution-dipping process from THF solutions.

A series of electroluminescence (EL) devices with the configuration of ITO/PEDOT:PSS/polymer (**P4** or its H-bonded dendrimers complexes)/BCP/Alq_3/LiF/Al were made, where BCP (i.e., 2,9-dimethyl-4,7-diphenyl-1,10-phenanthroline) was used as a hole-blocking layer and Alq_3 (i.e., tris(8-hydroxyquinoline)aluminum) was used as an electron-transporting layer. ITO substrates, where

glass substrates were coated with indium−tin oxide (ITO) having a sheet resistance of ∼20 Ω/square and an effective individual device area of 3.14 mm^2, were routinely cleaned by ultrasonic treatments in detergent solutions and diluted water, followed by rinsing with acetone and then ethanol. After drying, ITO substrates were kept in oxygen plasma for 4 min before being loaded into the vacuum chamber. The poly(3,4-ethylenedioxythiophene):poly(styrenesulfonate) (PEDOT:PSS) films were first deposited on precleaned ITO substrates by spin-coating at 6000 rpm for 1 min and subsequently cured in an oven at 120 °C for 1 h. Then, light-emitting polymers (**P4** or its H-bonded side-chain dendritic complexes) in THF solutions (10 mg/mL) were spin-coated onto the PEDOT:PSS layer at 4000−5500 rpm. The thicknesses of PEDOT:PSS and LED polymers were measured by an Alfa Step 500 surface profiler (Tencor). BCP and Alq_3 were thermally deposited at a rate of 1−2 Å/s under a pressure of $\sim 2 \times 10^{-5}$ Torr in an Ulvac cryogenic deposition system. Under the same deposition condition, one layer of LiF was thermally deposited as a cathode at a rate of 0.1−0.2 Å/s, which was followed by capping with aluminum. The current−voltage−luminescence characteristics were measured in ambient condition by a Keithley 2400 source meter and a Newport 1835C optical meter equipped with an 818ST silicon photodiode.

Materials. Chemicals and solvents were reagent grades and purchased from Aldrich, ACROS, TCI, and Lancaster Chemical Co. Tetrahydrofuran (THF) and triethylamine (Et_3N) were distilled to keep anhydrous before use. Azobis(isobutyronitrile) (AIBN) was recrystallized from methanol before use. The other chemicals were used without further purification. Different generations of dendritic H-donors (**G1COOH**−**G3COOH**), as shown in Figure 1, used in H-bonded side-chain dendritic complexes were reported in our previous work.[37] 10-Bromodecanol,[39] 1,3-dichloro-1,1,3,3-tetrabutyldistannoxane,[40] and monomer **CAZ (M2)**[41] were prepared by following the already published procedures.

4-Iodo-2,5-dimethoxybenyl Alcohol (2). To a stirred solution of 4-iodo-2,5-dimethoxybenzaldehyde, **1** (8.0 g, 27.4 mmol), in 200 mL of THF/MeOH (1:1), $NaBH_4$ (0.52 g, 13.7 mmol) was added very slowly to react at room temperature. After 1 h, the solution was cooled to 0 °C by ice bath, acidified with dilute HCl solution, and extracted with ethyl acetate. The resulting materials in organic phase were combined and washed with water. Afterward, the organic extracts were dried over Na_2SO_4 and evaporated. The purified residue was recrystallized from dichloromethane/2-propanol to give a colorless crystal. Yield: 7.6 g (95%). ^{1}H NMR (300 MHz, $CDCl_3$): δ (ppm) 7.25 (s, 1H), 6.85 (s, 1H), 4.65 (d, J = 6.3 Hz, 2H), 3.85 (s, 3H), 3.82 (s, 3H), 2.22 (t, J = 6.6 Hz, 1H).

1-Iodo-4-chloromethyl-2,5-dimethoxybenzene (3). To a stirred solution of **2** (7.0 g, 23.8 mmol) in 1,4-dioxane (200 mL), concentrated HCl (20 mL) was added to reflux for 10 h. After the reaction was completed, the crude mixture was added with water. The organic layer was extracted with ethyl acetate, dried over Na_2SO_4, and evaporated. The residual product was purified by flash column chromatography (silica gel, *n*-hexane/ethyl acetate 40:1) to give a white solid. Yield: 6.8 g (92%). ^{1}H NMR (300 MHz, $CDCl_3$): δ (ppm) 7.29 (s, 1H), 6.86 (s, 1H), 4.60 (s, 2H), 3.85 (s, 3H), 3.83 (s, 3H).

4-Iodo-2,5-dimethoxybenzyldiethylphosphonate (4). Compound **3** (6.0 g, 19.2 mmol) was mixed with an excess of triethyl phosphite (20 mL), and the mixture was heated to reflux and reacted for 12 h. The excess of triethyl phosphite was removed under reduced pressure, and the crude product was purified by washing with hot hexane to give a white solid. Yield: 7.2 g (90%). ^{1}H NMR (300 MHz, $CDCl_3$): δ (ppm) 7.25 (s, 1H), 6.9 (s, 1H), 4.08−3.99 (m, 4H), 3.83 (s, 3H), 3.80 (s, 3H), 3.20 (d, J = 21.6 Hz, 2H), 1.24 (t, 6.9 Hz, 6H).

1-Iodo-2,5-dimethoxy-4-[2-(4-pyridyl)ethenyl]benzene (5). To a solution of pyridine-4-carboxaldehyde (1.86 g, 17.4 mmol) in anhydrous THF (10 mL), a suspension of **4** (6.0 g, 14.5 mmol) and *t*-BuOK (2.93 g, 26.1 mmol) in anhydrous THF (60 mL) under nitrogen was slowly added. The mixture was stirred to react at room temperature for 12 h. After the reaction was completed, it was quenched with water and extracted with dichloromethane. After that, the organic layer was dried over Na_2SO_4 and evaporated. The crude product was purified by column chromatography (silica gel, dichloromethane/acetone 30:1) to give a yellow solid. Yield: 3.2 g (60%). ^{1}H NMR (300 MHz, $CDCl_3$): δ (ppm) 8.55 (d, J = 4.5 Hz, 2H), 7.57 (d, J = 16.5 Hz, 1H), 7.37 (d, J = 4.5 Hz, 2H), 7.30 (s, 1H), 7.01 (d, J = 16.5 Hz, 1H), 7.00 (s, 1H), 3.88 (s, 3H), 3.84 (s, 3H).

10-(4-Bromophenoxy)decan-1-ol (6). To a stirred solution of 4-bromophenol (4.0 g, 23.1 mmol) in acetone (200 mL), potassium carbonate (9.6 g, 69.3 mmol), 10-bromodecanol (6.6 g, 27.7 mmol), and a few amounts of potassium iodide (ca. 10 mg) were added to reflux for 48 h under nitrogen. After cooling to room temperature, the solvent was removed under reduced pressure, and the residue was taken up in water and extracted with ethyl acetate. Next, the organic layer was dried over Na_2SO_4 and evaporated. The crude product was purified by column chromatography (silica gel, *n*-hexane/ethyl acetate 3:1) to give a white solid. Yield: 6.1 g (80%). ^{1}H NMR (300 MHz, $CDCl_3$): δ (ppm) 7.33 (d, J = 9.0 Hz, 2H), 6.75 (d, J = 9.0 Hz, 2H), 3.89 (t, J = 6.3 Hz, 2H), 3.62 (t, J = 6.6 Hz, 2H), 1.78−1.69 (m, 2H), 1.59−1.50 (m, 2H), 1.41−1.29 (m, 12H).

4-[4-(10-Hydroxydecyloxy)phenyl]-2-methyl-3-butyn-2-ol (7). A solution of **6** (4.0 g, 12.1 mmol), PPh_3 (63.1 mg, 0.24 mmol), and CuI (45.6 mg, 0.24 mmol) in dry Et_3N (80 mL) was degassed with nitrogen for 5 min. Then, the solution was added with 2-methyl-3-butyn-2-ol (2.0 g, 24.2 mmol) and $Pd(PPh_3)_2Cl_2$ (84.1 mg, 0.12 mmol) at room temperature, and the reaction mixture was stirred to react at 70 °C for 12 h. The mixture was filtered, and the solvent was removed in vacuum. The crude mixture was extracted using ethyl acetate, and the extract was washed with water, dried over Na_2SO_4, and then evaporated. Subsequently, the crude product was purified by column chromatography (silica gel, *n*-hexane/ethyl acetate 1:1) to give a light yellow solid. Yield: 3.14 g (78%). ^{1}H NMR (300 MHz, $CDCl_3$): δ (ppm) 7.31 (d, J = 9.0 Hz, 2H), 6.79 (d, J = 9.0 Hz, 2H), 3.92 (t, J = 6.6 Hz, 2H), 3.62 (t, J = 6.6 Hz, 2H), 1.77−1.70 (m, 2H), 1.60 (s, 6H), 1.58−1.50 (m, 2H), 1.42−1.29 (m, 12H).

4-Ethynyl-1-(10-hydroxydecan-1-yloxy)benzene (8). A stirred solution of **7** (2.5 g, 7.5 mmol) and finely powdered KOH (1.26 g, 22.5 mmol) in 1,4-dioxane (80 mL) was refluxed under nitrogen for 3 h. After cooling to room temperature, the solvent was removed under reduced pressure and the residue was taken up in water, and then the mixture was extracted with ethyl acetate and acidified with 3 N HCl (150 mL). The organic solution was washed with water, dried over Na_2SO_4, and then evaporated. Afterward, the crude product was purified by column chromatography (silica gel, *n*-hexane/ethyl acetate 5:1) to give a light yellow solid. Yield: 1.75 g (85%). ^{1}H NMR (300 MHz, $CDCl_3$): δ (ppm) 7.39 (d, J = 9.0 Hz, 2H), 6.80 (d, J = 9.0 Hz, 2H), 3.92 (t, J = 6.6 Hz, 2H), 3.62 (t, J = 6.6 Hz, 2H), 2.97 (s, 1H), 1.80−1.70 (m, 2H), 1.57−1.50 (m, 2H), 1.42−1.29 (m, 12H).

1-{[4-(10-Hydroxydecyloxy)phenyl]ethynyl}-2,5-dimethoxy-4-[2-(4-pyridyl)ethenyl]benzene (9). A solution of **5** (1.0 g, 2.72 mmol), **8** (0.78 g, 2.85 mmol), and PPh_3 (14.1 mg, 0.054 mmol) in 80 mL of dry Et_3N/THF (1:1) was degassed with nitrogen for 5 min. Then, the solution was added with CuI (10.3 mg, 0.054 mmol) and $Pd(PPh_3)_2Cl_2$ (19.1 mg, 0.027 mmol) at room temperature, and it was stirred to react at 50 °C overnight. The mixture was filtered, and the solvent was removed in vacuum. The crude mixture was extracted using dichloromethane, and the extract was washed with water, dried over Na_2SO_4, and then evaporated. After that, the crude product was purified by column chromatography (aluminum oxide, dichloromethane/acetone 40:1) to give a yellow solid. Yield: 1.28 g (92%). ^{1}H NMR (300 MHz, $CDCl_3$): δ (ppm) 8.56 (d, J = 4.5 Hz, 2H), 7.66 (d, J = 16.5 Hz, 1H), 7.50 (d, J = 9.0 Hz, 2H), 7.39 (d, J = 4.5 Hz, 2H), 7.11 (s, 1H), 7.04 (d, J = 16.5 Hz, 1H), 7.04 (s, 1H), 6.87 (d, J = 9.0 Hz, 2H), 3.99 (t, J = 6.6 Hz, 2H), 3.97 (s, 3H), 3.89 (s, 3H), 3.62 (t, J = 6.6 Hz, 2H), 1.81−1.72 (m, 2H), 1.57−1.51 (m, 2H), 1.41−1.30 (m, 12H).

1-{[4-(10-Methacryloyloxydecyloxy)phenyl]ethynyl}-2,5-dimethoxy-4-[2-(4-pyridyl)ethenyl]benzene, PBB (M1). To a Schlenk tube, compound **9** (1.0 g, 1.95 mmol), vinyl methacrylate (0.55 g, 4.88 mmol), 1,3-dichloro-1,1,3,3-tetrabutyldistannoxane (43.12 mg, 0.078 mmol), and 2,6-di-*tert*-butyl-4-methylphenol (25.78 mg, 0.117 mmol) in dry THF (2 mL) were purged with nitrogen for 15 min at room temperature. The tube was sealed and heated with stirring at 50 °C for 2 days. After cooling to room temperature, the reaction mixture was extracted using dichloromethane, and the extract was washed with water, dried over Na_2SO_4, and then evaporated. The crude product was purified by column chromatography (aluminum oxide, *n*-hexane/dichloromethane 1:1) and then washed with hexane to give a light yellow solid. Yield: 0.97 g (85%). ^{1}H NMR (300 MHz, $CDCl_3$): δ (ppm) 8.57 (d, $J = 4.5$ Hz, 2H), 7.66 (d, $J = 16.5$ Hz, 1H), 7.50 (d, $J = 9.0$ Hz, 2H), 7.39 (d, $J = 4.5$ Hz, 2H), 7.11 (s, 1H), 7.04 (d, $J = 16.5$ Hz, 1H), 7.04 (s, 1H), 6.87 (d, $J = 9.0$ Hz, 2H), 6.10 (s, 1H), 5.55 (s, 1H), 4.14 (t, $J = 6.6$ Hz, 2H), 3.97 (t, $J = 6.6$ Hz, 2H), 3.96 (s, 3H), 3.89 (s, 3H), 3.62 (t, $J = 6.6$ Hz, 2H), 1.95 (s, 3H), 1.81−1.75 (m, 2H), 1.58−1.53 (m, 2H), 1.42−1.30 (m, 12H). HRMS (EI): calcd for $C_{37}H_{43}NO_5$, 581.3141; found 581.3146. Anal. Calcd for $C_{37}H_{43}NO_5$: C, 76.39; H, 7.45; N, 2.41. Found: C, 76.15; H, 7.37; N, 2.44.

General Procedure for the Syntheses of Homopolymers and Copolymers (P1−P5). All polymerization procedures were carried out according to the free radical polymerization described by the following steps. To a Schlenk tube, 1.5 g of monomers **M1**, **M2**, or the mixture of **M1** and **M2** was dissolved in dry THF (7.5 mL) with 20 wt % of monomer concentration and AIBN (2 mol % of total monomer concentration) as an initiator. The solution was degassed by three freeze−pump−thaw cycles and then sealed off. The reaction mixture was stirred and heated at 60 °C for 24 h. After polymerization, the polymer was precipitated into diethyl ether. Then, the precipitated polymer was collected, washed with diethyl ether, and dried under high vacuum.

P1 (HPBB). ^{1}H NMR (300 MHz, DMSO-d_6): δ (ppm) 8.44 (br, 2H), 7.53−6.77 (br, 10H), 3.80 (br, 10H), 1.66−1.24 (br, 21H).

P2 (PBB-CAZ$_1$). ^{1}H NMR (300 MHz, DMSO-d_6): δ (ppm) 8.46 (br, 2H), 7.97−6.75 (br, 18H), 3.88 (br, 14H), 1.43−1.08 (br, 26H).

P3 (PBB-CAZ$_5$). ^{1}H NMR (300 MHz, DMSO-d_6): δ (ppm) 8.48 (br, 2H), 7.92−6.76 (br, 50H), 4.33−3.83 (br, 30H), 1.43−0.06 (br, 46H).

P4 (PBB-CAZ$_9$). ^{1}H NMR (300 MHz, DMSO-d_6): δ (ppm) 8.48 (br, 2H), 7.88−6.76 (br, 80H), 4.34−3.83 (br, 45H), 1.43−0.16 (br, 65H).

P5 (HCAZ). ^{1}H NMR (300 MHz, DMSO-d_6): δ (ppm) 7.89 (br, 2H), 7.32−7.00 (br, 6H), 4.34−3.94 (br, 4H), 0.99−0.15 (br, 5H).

Sample Preparation of Supramolecular Side-Chain Copolymers (i.e., H-Bonded Side-Chain Dendritic Complexes). H-bonded side-chain dendritic complexes were made of appropriate (fully H-bonded) molar ratios of H-acceptor copolymers (**P3** and **P4**) and dendritic H-donors (**G1COOH**−**G3COOH**) in THF solutions, and then the solvent was removed by slow evaporation and followed by drying under vacuum at 50 °C.

Results and Discussion

Syntheses and Characterization of Polymers. The synthetic routes of monomer **PBB (M1)** and polymers **P1**−**P5** are shown in Scheme 1. The starting material **1** (i.e., 4-iodo-2,5-dimethoxybenzaldehyde) was synthesized by following a reported procedure[42] via iodination of 2,5-dimethoxybenzaldehyde with iodine and silver nitrate in the presence of methanol. The aldehyde group of compound **1** was further reduced to a benzyl alcohol and then was transformed into a benzyl chloride group with hydrochloric acid in the presence of 1,4-dioxane to give compound **3**, which was converted to the corresponding phosphonate ester **4** by Michaelis−Arbuzov reaction under the triethyl phosphite treatment with a yield of 90%.[43] Compound **5** was prepared by means of Horner−Wadsworth−Emmons (HWE) olefination reaction between compound **4** and pyridine-4-carboxaldehyde using potassium *tert*-butoxide as a base in THF to give 60% yield.[44] Compound **6** in 80% yield was obtained by reaction of 4-bromophenol with 10-bromodecanol under Williamson etherification condition (K_2CO_3/acetone). The latter Sonogashira (Pd-catalyzed) coupling reaction of compound **6** with 2-methyl-3-butyn-2-ol afforded compound **7** in the presence of a catalytic amount (1 mol %) of $Pd(PPh_3)_2Cl_2$ in Et_3N with a yield of 78%,[45] which was then deprotected with KOH/1,4-dioxane to acquire compound **8** in 85% yield. Subsequently, the three-conjugated rings of compound **9** with a yield of 92% was prepared through a second Sonogashira coupling reaction between compounds **8** and **5** in Et_3N/THF (1:1). Finally, monomer **PBB (M1)** with a high yield of 85% was obtained by transesterification reaction[46] between compound **9** and an excess amount (2.5 equiv) of vinyl methacrylate in the presence of a higher concentration of 1,3-dichloro-1,1,3,3-tetrabutyldistannoxane as a catalyst and 2,6-di-*tert*-butyl-4-methylphenol as an inhibitor in THF. The yield is much better than that reported[47] by our previous esterification reaction. The final chemical structure of monomer **PBB (M1)** was confirmed by ^{1}H NMR spectroscopy, HRMS, and elemental analysis (see Experimental Section and Supporting Information).

Table 1. Composition, Yields, Molecular Weights, and Degradation Temperatures of Polymers P1−P5

polymer	molar ratio: feed monomer (**PBB/CAZ**)	molar ratio: polymers (x/y)[a]	yield (%)	M_w (g/mol)[b]	PDI (M_w/M_n)[b]	T_d (°C)[c]
P1 (HPBB)	1/0	1/0	73	14 400	1.72	357
P2 (PBB-CAZ$_1$)	1/1	1/1	88	38 100	3.24	323
P3 (PBB-CAZ$_5$)	1/5	1/5	85	45 600	2.99	305
P4 (PBB-CAZ$_9$)	1/10	1/9	81	53 100	3.69	300
P5 (HCAZ)	0/1	0/1	75	47 800	3.65	276

[a] Determined by ^{1}H NMR spectra. [b] Weight-average molecular weight (M_w) and polydispersity index (PDI) determined by GPC in THF using polystyrene as a standard. [c] Temperature (°C) at 5% weight loss measured by TGA at a heating rate of 20 °C min^{-1} under nitrogen.

The polymerization reactions with good yields (ranging 73−88%) were carried out in THF at 60 °C through free radical polymerization in the presence of azobis(isobutyronitrile) (AIBN) as an initiator. The feeding ratios of monomers **PBB (M1)** to **CAZ (M2)** were 1:0, 1:1, 1:5, 1:10, and 0:1, respectively, to acquire H-acceptor polymers **P1**−**P5**. The chemical structures of polymers **P1**−**P5** in DMSO-d_6 were verified by ^{1}H NMR spectroscopy in comparison with those of their monomers **PBB (M1)** and **CAZ (M2)** (see Supporting Information). In the ^{1}H NMR spectra of polymers, the disappearance of proton peaks in the region of vinyl (methacrylate) groups with chemical shifts at 5.4−6.1 ppm indicated that all monomers were reacted. The copolymer compositions were estimated by comparing the relative integration areas of the peaks at 8.5 ppm (corresponding to two protons of α-pyridyl groups in **PBB**) and 6.7−7.9 ppm (corresponding to the other overlapped aromatic protons of **PBB** and **CAZ** units), respectively. Regarding the compositions of copolymers **P2**−**P4**, the actual compositions of **P2** and **P3** are very close to the feeding ratios of monomers, except that **P4** has a slightly lower molar ratio than that of feeding. All polymers are soluble in common organic solvents, such as THF, DMSO, and DMF. The weight-average molecular weights (M_w) and polydispersity indexes (PDI) of polymers **P1**−**P5**, determined by gel permeation chromatography (GPC) with THF as the eluting solvent and polystyrene as standards, are in the range 14 400−53 100 g/mol and 1.72−3.69, respectively. The compositions (input and output molar ratio), molecular weights (M_w), PDI values, and yields of polymers **P1**−**P5** are summarized in Table 1.

The existence of hydrogen bonds in the H-bonded complexes can be confirmed by FTIR spectroscopy. Therefore, the IR spectra (at room temperature) of H-acceptor polymer **P3**,

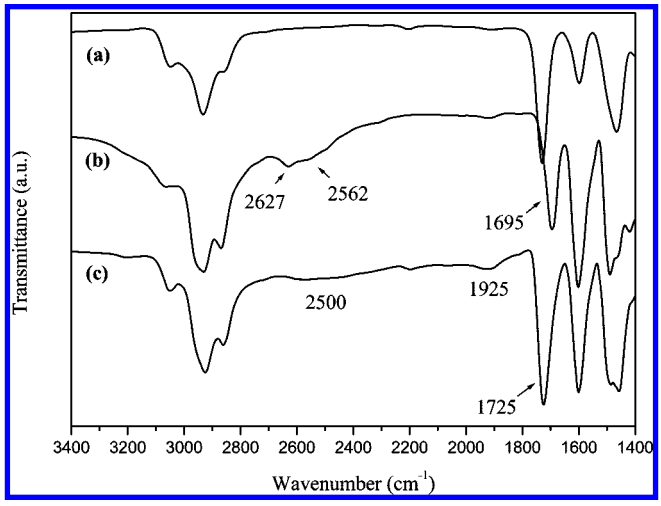

Figure 3. FTIR spectra of (a) H-acceptor polymer **P3 (PBB-CAZ$_5$)**, (b) dendritic H-donor **G1COOH**, and (c) H-bonded side-chain dendritic complexes **P3/G1COOH** at room temperature.

H-donor **G1COOH**, and H-bonded side-chain dendritic complexes (side-chain copolymers with pendent dendrimers) **P3/G1COOH** shown in Figure 3 are compared to analyze the formation of hydrogen bonds between H-acceptor polymer **P3** and H-donor dendrimer **G1COOH**. In contrast to the O−H bands of pure H-donor (H-bonded dendritic dimer) **G1COOH** at 2627 and 2562 cm^{-1}, the weaker O−H bands observed at 1925 and 2500 cm^{-1} in the H-bonded side-chain dendritic complex **P3/G1COOH** are indicative of stronger hydrogen bonding between the pyridyl groups of polymer **P3** and the carboxylic acid of **G1COOH** in the H-bonded complex. On the other hand, a stretching vibration of C═O at 1695 cm^{-1} in pure **G1COOH** is shifted toward higher wavenumber and overlapped with the band of the ester carbonyl groups at 1725 cm^{-1} in the H-bonded dendritic complex **P3/G1COOH**, which shows that the carbonyl group was in a less associated state than that in the pure H-bonded dimer state of H-donor **G1COOH**. These results suggest that hydrogen bonds were formed between **P3** and **G1COOH** in the solid state of the H-bonded dendritic complex **P3/G1COOH**. The other H-bonded complexes discussed in this study should have similar consequences as the demonstrated H-bonded complexes.[48]

Thermal Properties. The thermal stabilities of polymers **P1**−**P5** were evaluated by thermogravimetric analyses (TGA), and their corresponding data are also summarized in Table 1. The TGA analyses indicate that the degradation temperatures (T_d) of polymers with 5% weight loss (under nitrogen) are between 276 and 357 °C, and T_d values decrease with increasing the molar ratio of monomer **CAZ (M2)** monotonically. Hence, homopolymers **P1 (HPBB)** and **P5 (HCAZ)** have the highest and lowest thermal stabilities, respectively, which means that the carbazole unit of monomer **CAZ (M2)** is less stable than the light-emitting unit of **PBB (M1)** in polymers **P1**−**P5** (see Supporting Information).

The phase transition temperatures of polymers **P1**−**P5** and H-bonded side-chain dendritic complexes containing H-acceptor polymers **P2 (PBB-CAZ$_1$)**, **P3 (PBB-CAZ$_5$)**, and **P4 (PBB-CAZ$_9$)**, which were determined by differential scanning calorimetry (DSC) under nitrogen, are summarized in Table 2. Polymers **P1**−**P5** only show glass transition temperatures (T_gs), but without any melting and crystallization peaks. The T_g values of polymers **P1**−**P5** (ranging 63−142 °C) gradually increase as the **CAZ (M2)** molar ratio increases. Hence, higher T_g values of copolymers with higher **CAZ** contents can be originated from the contribution of the bulky carbazole pendent groups, where the mobility of polymeric chains are restricted due to the steric hindrance and rigidity of carbazole units.

Table 2. Glass Transition Temperatures of Polymers P1−P5 and H-Bonded Side-Chain Dendritic Complexes Containing H-Acceptor Polymers P2−P4

polymer or H-bonded complex	T_g (°C)	polymer or H-bonded complex	T_g (°C)
P1 (HPBB)	63	**P2/G3COOH**	−[a]
P2 (PBB-CAZ$_1$)	88	**P3/G1COOH**	81
P3 (PBB-CAZ$_5$)	117	**P3/G2COOH**	86
P4 (PBB-CAZ$_9$)	125	**P3/G3COOH**	83
P5 (HCAZ)	142	**P4/G1COOH**	88
P2/G1COOH	60	**P4/G2COOH**	99
P2/G2COOH	68	**P4/G3COOH**	89

[a] Omitted due to the possible unstabilized H-bonded structures originated from the highest steric hindrance between the highest generation of dendrimer **G3COOH** and the denser H-acceptor units in **P2**.

During the heating run of polarizing optical microscopy (POM) study in the glassy state of polymers, homopolymer **P1 (HPBB)** exhibited weak birefringent behavior (up to the clearing point of 125 °C) corresponding to a characteristic mesophase at 90 °C (see Supporting Information), which was further confirmed by powder X-ray diffraction (XRD). The diffraction pattern has two diffuse halos in the small- and wide-angle regions, respectively, indicating the absence of any positional order as a smectic or highly ordered phase.[49] Hence, these results suggest that the mesogenic homopolymer **P1** showed the nematic phase [glassy (64 °C) nematic (125 °C) isotropic]. However, only homopolymer **P1** formed the nematic phase, and the other polymers **P2**−**P5** do not have any mesogenic properties, which is probable that the incorporation of the bulky carbazole groups into the copolymer system will disturb the self-assembly of rigid rods in **PBB** units and thus to prohibit from their mesogenic behavior.

To elucidate the H-bonding effect on the thermal properties of supramolecular side-chain dendritic complexes, **OXD** dendritic H-donors (bearing benzoic acids) were introduced to be H-bonded with light-emitting H-acceptor copolymers **P2 (PBB-CAZ$_1$)**, **P3 (PBB-CAZ$_5$)**, and **P4 (PBB-CAZ$_9$)**, where **P2/G3COOH** is omitted due to the possible unstabilized H-bonded structures originated from the highest steric hindrance between the highest generation of dendrimer **G3COOH** and the denser H-acceptor units in **P2**. As shown in Table 2, both series of H-bonded side-chain dendritic complexes containing H-acceptor polymers **P3** and **P4** show only a single T_g, which suggests good miscibilities between **OXD** dendritic H-donors (i.e., **G1COOH**−**G3COOH**) and H-acceptor polymers (i.e., **P3** and **P4**). Besides, since no melting and crystallization were observed in the DSC measurements, it suggests that these H-bonded dendritic complexes possess amorphous characteristics. Moreover, neither phase separation nor mesogenic properties were observed in the POM measurements. However, the T_g values of supramolecular side-chain dendritic complexes (containing **P3** and **P4**) are notably lower than those of their H-acceptor copolymers (i.e., **P3** and **P4**). This result may be explained by that the free volumes of the H-bonded side-chain dendritic complexes were enhanced by the bulky dendritic structures of the **OXD** H-donors.

In comparison with different generations of H-bonded side-chain dendritic complexes containing **P3** and **P4** (i.e., **P3/G1COOH**−**G3COOH** and **P4/G1COOH**−**G3COOH**), both series of T_g values increase initially with enlarging the generation number of the **OXD** dendron from G1 to G2, reaching the highest values at dendrimer G2 (i.e., **P3/G2COOH** and **P4/G2COOH**). With the further increase of the generation number to dendrimer G3, both series of T_g values begin to decrease. The initial increase in the T_g value is probably due to the increase of the molecular weight in a larger dendron (from G1 to G2),

Table 3. Absorption and PL Emission Spectral Data of H-Acceptor Monomer M1 (PBB) and Polymers P1−P5 in THF Solutions and Solid Films

polymer	$\lambda_{abs,sol}$[a] (nm)	$\lambda_{PL,sol}$[a,b] (nm)	$\lambda_{PL,film}$[b] (nm)	$\Phi_{PL,sol}$[b,c]
M1 (PBB)	320, 385	445	495	0.52
P1 (HPBB)	320, 385	449	496	0.49
P2 (PBB-CAZ$_1$)	294, 320, 342, 385	447	487	0.68
P3 (PBB-CAZ$_5$)	294, 328, 342, 385	445	469	0.83
P4 (PBB-CAZ$_9$)	294, 328, 342, 385	444	466	0.94
P5 (HCAZ)	294, 328, 343	348, 364	352, 367	

[a] Measured in dilute THF solutions. [b] Excited at the maximum absorption of **PBB** units. [c] Solution fluorescence quantum efficiencies were measured in THF, relative to 9,10-diphenylanthracene (Φ_{PL} = 0.90).

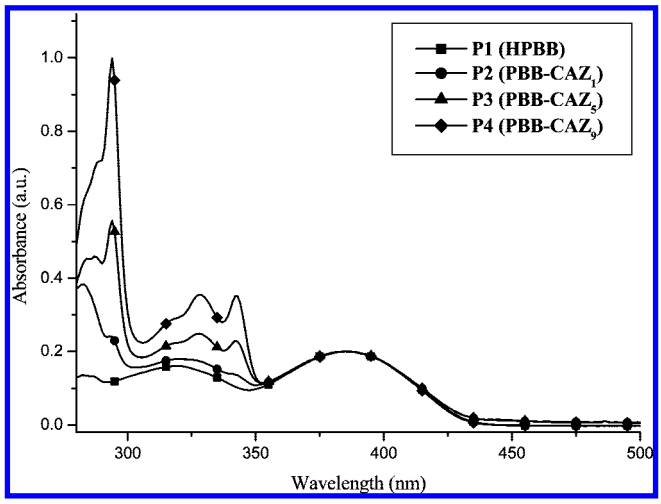

Figure 4. Absorption spectra of H-acceptor polymers **P1**−**P4** in THF solutions, normalized at the maximum absorption peak of the light-emitting **PBB** segments at 385 nm.

which is similar to the phenomena observed in our previous study of H-bonded dendrimers.[37] However, the further decrease in the T_g value of the highest generation number (G3) is due to the free volume effect (increasing with enlarging the size of the dendritic **OXD** wedges so as to decrease the adjacent polymeric chain interactions) being more dominant than the molecular weight effect, which was also described in our previous polyfluorene polymers containing **OXD** dendritic pendants.[50] Therefore, the competition between the free volume effect and the molecular weight effect influenced the T_g values of H-bonded side-chain dendritic complexes containing **P3** and resulted in the following order: **P3/G2COOH** > **P3/G3COOH** > **P3/G1COOH**. A similar tendency was also observed in analogous H-bonded dendritic complexes containing **P4**. However, there were some possibilities for unstabilized H-bonded structures of complexes made from the highest generation of dendrimer **G3COOH** and the denser H-acceptor units in **M1** and **P2** due to the steric hindrance within the higher generations of dendrimers and hence to induce the incomplete H-bonded complexes. Therefore, the decrease of T_g values in the complexes might be also attributed to the plasticizing effect of the non-H-bonded dendrimers, which were homogeneously dispersed in the complexes.

Optical Properties. The absorption and photoluminescence (PL) spectra of H-acceptor monomer **M1 (PBB)** and polymers **P1**−**P5** were measured in both solution and solid states, and their photophysical properties are summarized in Table 3. As shown in Figure 4, the absorption intensities of copolymers **P2**−**P4** at 294, 328, and 342 nm (in THF solutions) increase dramatically by raising the **CAZ** content, which are attributed to the absorption bands of the **CAZ** moieties. The additional absorption bands of polymers **P1**−**P4** at ca. 320 and 385 nm

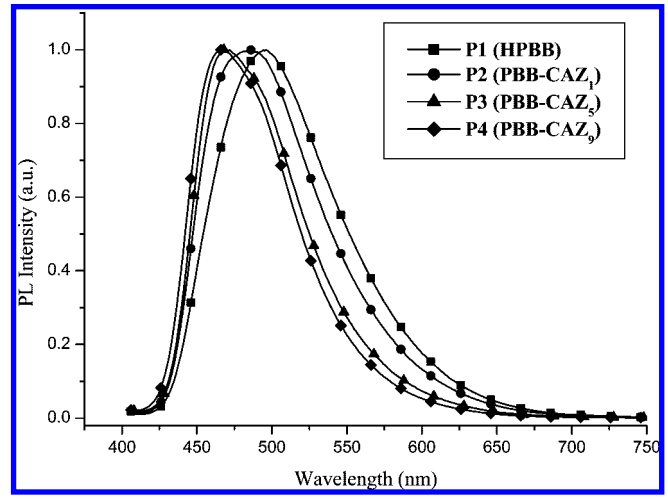

Figure 5. Normalized PL spectra of H-acceptor polymers **P1**−**P4** excited at the maximum absorption (397 nm) of the light-emitting **PBB** segments in solid films.

are assigned to the light-emitting **PBB** segments of the H-acceptor moieties. The copolymers do not demonstrate any new (or shifted) bands in the absorption spectra, indicating no interaction between the **CAZ** and **PBB** moieties in the ground state. The absorption spectra of the polymers in solid films are similar except for 5−7 nm of red shifts in contrast to those in THF solutions (see Supporting Information). The PL emission spectra of polymers **P1**−**P4** in solid films show 22−47 nm of significant red shifts, i.e., **P1** (47 nm) > **P2** (40 nm) > **P3** (24 nm) > **P4** (22 nm), in comparison with their corresponding dilute solutions (see Table 3), which is due to the formation of $\pi-\pi$ stacking and molecular aggregation in solid state. Furthermore, compared with copolymers **P2**−**P4** in solid films as shown in Figure 5, homopolymer **P1** exhibits the largest red shift, i.e., 47 nm, in PL spectra. With the increase of **CAZ** contents in copolymers **P2**−**P4**, the PL peaks are blue-shifted from 487 nm in **P2** to 466 nm in **P4**. This result clearly indicates that the dilution effect by the **CAZ** moieties can be incorporated into the copolymers to suppress the intermolecular $\pi-\pi$ stacking and the aggregation of the light-emitting **PBB** units in polymers and thus to reduce the red shifts (by aggregation) in the PL emission spectra. As listed in Table 3, the PL quantum yields (Φ_{PL}) of polymers **P1**−**P4** in solutions were in the order of **P1** < **P2** < **P3** < **P4**, where **P4** has the largest quantum yield (Φ_{PL} = 0.94) due to the highest content of **CAZ** moieties. This consequence indicates that the dilution effect of **CAZ** units in the copolymers will reduce the aggregation and self-quenching of the **PBB** segments to acquire higher PL quantum yields.

In order to investigate the generation effect of **OXD** dendrons on the absorption spectra of H-bonded side-chain dendritic complexes (in solid films), the absorption spectra of model compound **1** (containing an **OXD** unit, which is illustrated in the Supporting Information) in THF solution and H-acceptor polymer **P3** in solid state are compared.[37] As shown in the absorption spectra of Figure 6, the maximum absorption wavelength $\lambda_{max,abs}$ of model compound **1** in THF solution is ca. 305 nm (from **OXD** units) and that of H-acceptor polymer **P3** in solid state is ca. 296 nm (from **CAZ** units). Nevertheless, the major absorption bands of H-bonded side-chain dendritic complexes containing **P3** in solid films are dominated at ca. 296 nm (from **CAZ** units) with a shoulder at ca. 315 nm (from **OXD** units), which are originated from the combined absorption band of the **OXD** and **CAZ** moieties. The longer absorption band at ca. 397 nm is attributed to the characteristic absorption of the light-emitting **PBB** units. By increasing the generation number of the dendritic H-donors in the H-bonded side-

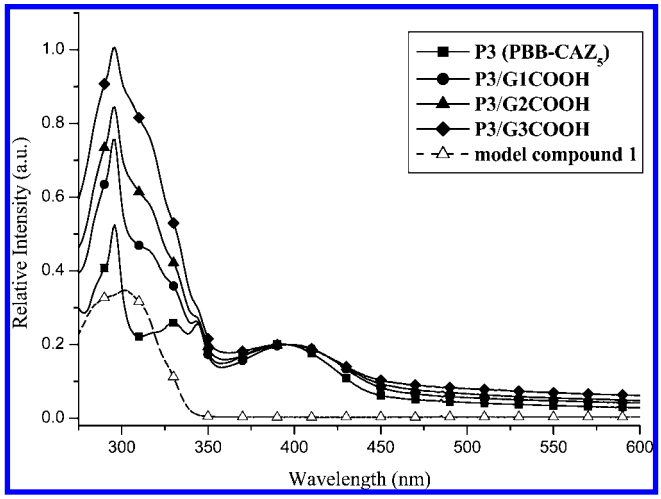

Figure 6. Absorption spectra of H-acceptor polymer **P3** and its H-bonded side-chain dendritic complexes in solid films normalized at the maximum absorption (397 nm) of the light-emitting **PBB** cores along with model compound **1** (containing an **OXD** unit with the maximum absorption around 305 nm in THF solution).

Table 4. Photophysical Properties of H-Bonded Side-Chain Dendritic Complexes Containing H-Acceptor Monomer M1 (PBB) and Polymers P2−P4

H-bonded complex	$\lambda_{PL,film}$ (nm)	$\Delta\lambda_{PL}$[a] (nm)	RFI[b]
M1/G1COOH	561	66	0.93
M1/G2COOH	555	60	1.25
M1/G3COOH	—[c]	—[c]	—[c]
P2/G1COOH	547	49	0.91
P2/G2COOH	536	46	1.76
P2/G3COOH	—[c]	—[c]	—[c]
P3/G1COOH	530	61	1.56
P3/G2COOH	520	51	2.16
P3/G3COOH	509	40	3.14
P4/G1COOH	523	57	2.09
P4/G2COOH	512	46	2.44
P4/G3COOH	498	32	4.45

[a] Different degrees of red-shifted PL emissions between the H-boned side-chain dendrimers and their corresponding H-acceptor copolymers. [b] Relative fluorescent intensities (RFI) were calculated by the ratios of the core emission intensities excited at the absorption peaks of the **OXD** units (305 nm) and the **PBB** cores (397 nm). [c] Omitted due to the possible unstabilized H-bonded structures originated from the highest steric hindrance between the highest generation of dendrimer **G3COOH** and the denser H-acceptor units in **M1** and **P2**.

chain dendritic complexes, the intensity of the absorption band in the **OXD** moieties at ca. 305−315 nm is proportional to the generation number of the H-donor dendrimers. The photophysical properties of H-bonded side-chain dendritic complexes containing H-acceptor monomer **M1 (PBB)** and polymers **P2−P4** in solid films are summarized in Table 4, where **M1/G3COOH** and **P2/G3COOH** are omitted due to the possible unstabilized H-bonded structures originated from the highest steric hindrance between the highest generation of dendrimer **G3COOH** and the denser H-acceptor units in **M1** and **P2**. From the results of Table 4, the least red-shifted PL emissions of $\Delta\lambda_{PL}$ in **P2/G1COOH** and **P2/G2COOH** have the evidence of the possible unstabilized H-bonded structures of complexes made from **P2**. Therefore, the possible unstabilized H-bonded structures of complexes made from **P2** will be similar to those made from **P1**, in which the H-bonded structures are possibly unsteady due to the steric hindrance between the denser H-acceptor units in **P1** (as well as **P2**) and the higher generation of dendrimers, especially for the highest generation of H-bonded complexes containing **G3COOH**.

The photophysical properties of both series of H-bonded side-chain dendritic complexes containing H-acceptor polymers **P3** and **P4** in solid films (see Table 4) are evaluated accordingly. Compared with H-acceptor polymer **P3 (PBB-CAZ5)** in Figure 7, the supramolecular side-chain dendritic complexes **P3/G1COOH−G3COOH** (excited at the maximum absorption of the light-emitting **PBB** units) exhibit red-shifted PL emissions with λ_{max} values at 530, 520, and 509 nm, respectively. This result is similar to our previous work[51] that red shifts of PL emissions are expected in the H-bonded structures, where the nonphotoluminescent H-donors bearing benzoic acids (as solid solvents) were H-bonded to the photoluminescent H-acceptors containing pyridyl groups. Therefore, analogous H-bonded side-chain dendritic complexes containing different generations of dendritic H-donors appeared to have different degrees of red-shifted PL emissions in comparison with H-acceptor polymer **P3**. The red shifts of PL emissions in H-bonded side-chain dendritic complexes **P3/G1COOH−G3COOH** are 61, 51, and 40 nm, respectively, where the higher generation of the H-bonded side-chain dendritic complex has a smaller red-shifted PL emission than the lower generation of the H-bonded side-chain dendritic complex. It clearly indicates that the larger dendritic wedges on the side chains have a larger site isolation or dendritic dilution effect than the smaller dendritic ones, so the higher generations of dendrimers efficiently minimize the interchain interaction and lower the aggregation extent between the light-emitting **PBB** units. The PL emission data of H-bonded dendritic dendrimers containing **P4** are also summarized in Table 4, which demonstrate similar trends as those of H-bonded dendritic dendrimers containing **P3**. However, in contrast to the same generation of **OXD** dendron, H-bonded dendritic complexes containing **P4** have smaller degrees of red-shifted PL emissions than H-bonded dendritic complexes containing **P3** (see Table 4). This might be due to the larger dilution effect of **CAZ** units in **P4 (PBB-CAZ9)** with higher **CAZ** contents than that in **P3 (PBB-CAZ5)**, where a higher **CAZ** molar ratio of **P4** reduces the interchain interaction between the light-emitting **PBB** units in these H-bonded side-chain dendritic complexes.

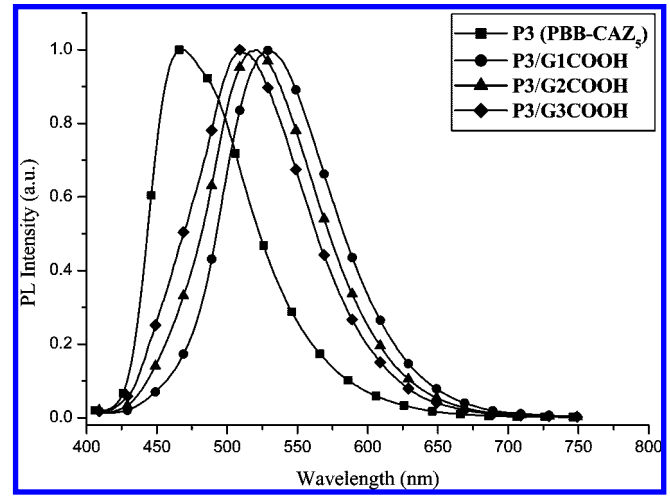

Figure 7. Normalized PL spectra of H-acceptor polymer **P3** and its H-bonded side-chain dendritic complexes excited at the maximum absorption (397 nm) of the light-emitting **PBB** cores in solid films.

Because of the significant spectral overlap in the absorption spectrum of homopolymer **P1** and the emission spectra of model compound **1** (containing an **OXD** unit) and homopolymer **P5** (as shown in the Supporting Information), the energy transfer from the **OXD** dendritic wedges and **CAZ** pendant groups to the light-emitting **PBB** cores can be expected. This effect was also probed by photoluminescent excitation (PLE) and absorption spectra of H-bonded side-chain dendritic complexes containing **P4** (see Figure 8). Similar spectral features of PLE spectra appear to match those of their corresponding absorption

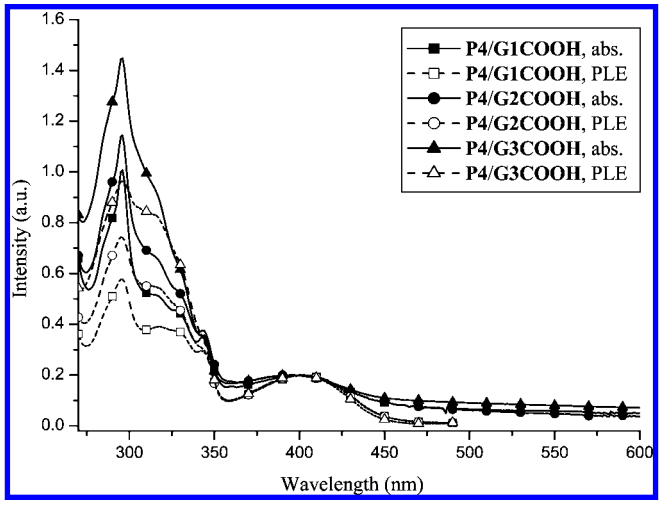

Figure 8. UV spectra and PLE spectra of H-acceptor polymer **P4** and its H-bonded side-chain dendritic complexes in solid films normalized at the light-emitting **PBB** units (397 nm), where PLE spectra were monitored at the corresponding maximum PL emissions.

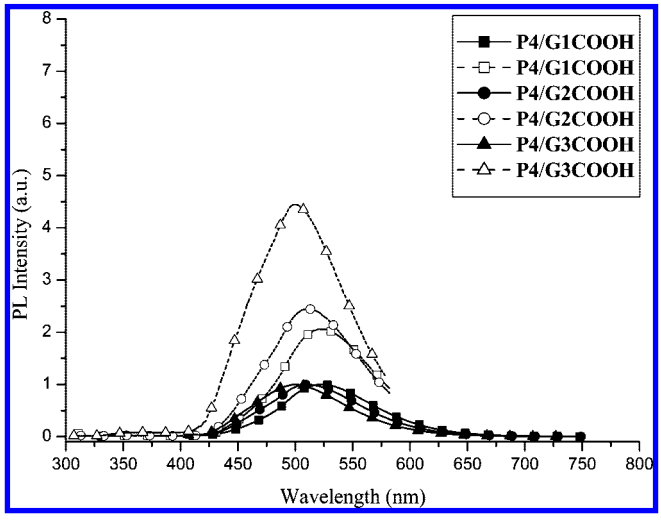

Figure 9. PL spectra of H-acceptor polymer **P4** and its H-bonded side-chain dendritic complexes in solid films, which were excited at the dendritic peripheral **OXD** units (at 305 nm for open symbols) and at the maximum absorption of the light-emitting **PBB** cores in H-bonded side-chain dendritic complexes containing dendritic H-donors (ca. 397 nm for solid symbols).

spectra, where PLE spectra were monitored at the corresponding maximum PL emission. This result indicates that the existing sites of **CAZ** pendent groups, peripheral **OXD** dendritic wedges, and light-emitting **PBB** cores (ca. 296, 305, and 397 nm, respectively) in such supramolecular side-chain dendrimers provide the characteristics of light-harvesting capability, i.e., antenna effect. Since only the energy transfer of the dendritic **OXD** units in the H-bonded side-chain dendritic complexes is concerned, the excitation wavelength of 305 nm was chosen at the maximum absorption of the dendritic **OXD** units. As shown in Figure 9, different generations of H-bonded dendritic complexes containing **P4** (**P4/G1COOH**−**G3COOH**) have PL emissions at wavelengths of 545, 539, and 522 nm, respectively. Upon excitation of the dendritic **OXD** units at 305 nm, H-bonded dendritic complexes apparently generated identical predominant emission peaks as those excited at the maximum absorption of the **PBB** cores. Whereas, no major PL emission from **OXD** dendrons was detected, and thus an efficient energy transfer from the peripheral **OXD** units to the **PBB** cores is confirmed. Furthermore, the functionalized **OXD** dendritic units

Table 5. Electrochemical Properties of H-Acceptor Polymer P4 and Its H-Bonded Side-Chain Dendritic Complexes

polymer or H-bonded complex	optical band gap[a] (eV)	$E_{ox/onset}$[b] (V)	HOMO (eV)	LUMO[c] (eV)
P4 (PBB-CAZ$_9$)	2.79	1.24	−5.64	−2.85
P4/G1COOH	2.75	1.26	−5.66	−2.91
P4/G2COOH	2.76	1.27	−5.67	−2.91
P4/G3COOH	2.77	1.27	−5.67	−2.90

[a] Estimated from the onset wavelength of optical absorption in solid films. [b] The onset oxidation potential vs SCE. [c] LUMO values were estimated by the deduction of optical band gaps from HOMO values.

or the light-emitting **PBB** cores can be independently addressed by changing the excitation wavelengths in PL experiments. By excitation of the electron-transporting dendrons and the light-emitting cores selectively, it provides a window to study the photoinduced energy transfer between proton donors and acceptors.

In addition, different generations of **OXD** dendritic H-donors were investigated to evaluate their antenna effect in the supramolecular side-chain dendrimers. Thus, the values of relative fluorescent intensities (RFI) in H-bonded side-chain dendritic complexes were calculated from the intensity ratios of their **PBB** core emissions by respective excitations at the maximum absorption peaks of the **OXD** dendrons (by the sensitized absorption at 305 nm and then energy transfer to **PBB** core emissions) and the maximum absorption peaks of the **PBB** cores (by the direct core absorption at 397 nm), respectively. The RFI values of H-bonded side-chain dendrimers containing H-acceptor copolymer **P4** and H-donor dendrimers **G1COOH** to **G3COOH** are 2.09, 2.44, and 4.45, respectively (as shown in Figure 9 and Table 4), which indicates that the intensity of the sensitized emission (by the energy transfer from **OXD** dendritic absorption at 305 nm) is even stronger than that of the direct **PBB** core emission (by the direct core absorption at 397 nm) in the H-bonded side-chain dendrimers. Therefore, the RFI values are much enhanced in the higher generations of H-bonded dendritic complexes (with the maximum values in both series of H-bonded side-chain dendritic complexes bearing the highest generation of H-donor dendrimer **G3COOH**), which is attributed to the higher absorptions by the larger numbers of **OXD** units in the higher generations of dendritic wedges as well as the further reduced aggregation of the light-emitting **PBB** cores by the more bulky sizes of dendrons in the higher generations of **OXD** H-donors.

Electrochemical Properties. The electrochemical behavior of H-acceptor copolymer **P4** and its H-bonded side-chain dendritic complexes were investigated by cyclic voltammetry (CV), and the results are summarized in Table 5. The highest occupied molecular orbital (HOMO) and lowest unoccupied molecular orbital (LUMO) levels were calculated according to the following equation: $E_{HOMO}/E_{LUMO} = -e(E_{ox/onset}/E_{red/onset} + 4.4)$ (eV).[52] The onset potentials were determined from the intersections of two tangents drawn at the rising and background currents of the CV curves. Since the onsets of the oxidation potentials (i.e., $E_{ox/onset}$) for H-acceptor copolymer **P4** and its H-bonded dendritic complexes were obtained from the CV measurements, the HOMO (i.e., E_{HOMO}) values were calculated from the previous equation, i.e., $E_{HOMO} = -e(E_{ox/onset} + 4.4)$ (eV), where $E_{ox/onset}$ is the onset oxidation potential versus the saturated calomel electrode (SCE). H-acceptor copolymer **P4** and its H-bonded dendritic complexes show the onset potentials of oxidation between 1.24 and 1.27 V in the anodic scans (see Table 5). The reduction potential peaks of H-acceptor copolymer and H-bonded side-chain dendrimers were not observed in the CV measurements, so crude estimations of LUMO values in the reduction processes of H-acceptor copolymer **P4** and its H-bonded side-chain dendrimers were made by the deduction

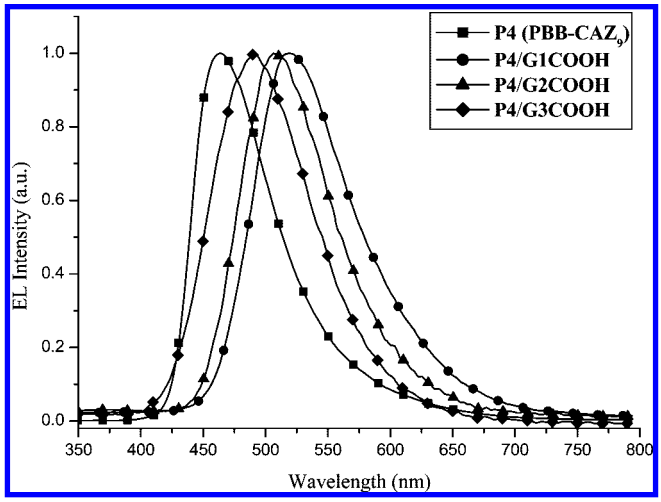

Figure 10. Normalized EL spectra of PLED devices with the configuration of ITO/PEDOT:PSS/polymer (**P4** or its H-bonded side-chain dendritic complexes)/BCP/Alq_3/LiF/Al.

of optical band gap values from HOMO values. The optical band gaps estimated from the absorption onsets of H-acceptor copolymer **P4** and its H-bonded side-chain dendritic complexes in solid films are also listed in Table 5, which reveals that H-acceptor copolymer **P4** has a larger band gap than its H-bonded side-chain dendrimers. Comparing the H-bonded side-chain dendritic complexes with various generations of **OXD** dendritic wedges, their LUMO values are not remarkably changed. However, it seems that the H-bonded side-chain dendritic complexes have slightly lower LUMO values than H-acceptor copolymer **P4** similar to a previously reported consequence.[50a]

Electroluminescence (EL) Properties. The electrochemical properties as well as the HOMO and LUMO energy levels of H-acceptor copolymer **P4** and its H-bonded side-chain dendritic complexes are crucial parameters for the device configuration and further confine the electron−hole recombination zone to the emission layer sufficiently. Therefore, H-acceptor polymer **P4** and its H-bonded dendritic complexes were fabricated into four-layer PLED devices, with a configuration of ITO/PEDOT:PSS (50 nm)/polymer (**P4** or its H-bonded dendritic complexes) (55−70 nm)/BCP (10 nm)/Alq_3 (30 nm)/LiF (1 nm)/Al (150 nm) using standard procedures of spin-coating and vacuum deposition methods, where polymer (**P4** or its H-bonded dendritic complexes) was used as the emission layer and PEDOT:PSS as the hole transporting layer (anode buffer). Besides, BCP (HOMO = −6.70 eV, LUMO = −3.20 eV), Alq_3 (HOMO = −6.00 eV, LUMO = −3.30 eV), and LiF/Al were employed as a hole-blocking layer, an electron-transporting layer, and a bilayer cathode, respectively. As shown in Figure 10, under forward bias voltages, the electroluminescence (EL) spectra of H-acceptor polymer **P4** and its H-bonded dendritic complexes show EL emissions in the range of 464−519 nm, indicating that the emission color can be effectively tuned from blue to green by incorporating light-emitting H-acceptor copolymer **P4** with various generations of **OXD** dendritic donors into the supramolecular side-chain polymer structures. These EL features are similar to those observed with corresponding PL emissions of the respective solid films. The electroluminescence (EL) properties of the PLED devices are summarized in Table 6, and their current−voltage and luminescence−voltage characteristics are displayed in Figure 11. A comparison of their turn-on voltages, the PLED device bearing H-bonded dendritic complex **P4/G1COOH**, has a lower turn-on voltage than that bearing H-acceptor **P4**. From this result, it can be concluded that the integration of **OXD** dendritic wedges (electron-transporting) into the supramolecular structures can remarkably improved device performance with a reduced turn-on voltage (though with a lower power efficiency). However, with higher generations (from **G1COOH** to **G3COOH**) of **OXD** dendritic wedges in the supramolecular H-bonded dendritic complexes, the turn-on voltages and power efficiencies of the PLED devices become worse (higher). This may be due to the intrinsic insulation properties of the higher generations of the **OXD** dendritic wedges with more 2-ethylhexyloxy end groups (as a shielding effect for electron and hole transporting) which consequently deteriorate the charge-carrier transporting properties and lead to higher turn-on voltages.[53] In addition, the PLED device bearing H-bonded dendritic complex **P4/G1COOH** has the best EL performance characteristics with a maximum luminance and luminous efficiency of 408 cd/m^2 at 18 V and

Table 6. Electroluminescence (EL) Device Performance Characteristics of H-Acceptor Polymer P4 and Its H-Boned Side-Chain Dendritic Complexes[a]

polymer or H-bonded complex	$\lambda_{EL,film}$ (nm)	V_{on}[b] (V)	luminance efficiency[c] (cd/A)	power efficiency[c] (lm/W)	max luminance (cd/m^2) (V)
P4 (PBB-CAZ$_9$)	464	8.5	0.75	0.109	947 (24)
P4/G1COOH	519	6.5	0.39	0.070	408 (18)
P4/G2COOH	506	7	0.11	0.034	242 (19.5)
P4/G3COOH	492	8.5	—[d]	—[d]	58 (22)

[a] Device configuration: ITO/PEDOT:PSS/polymer (**P4** or its H-bonded side-chain dendritic complexes)/BCP/Alq_3/LiF/Al. [b] V_{on}: the turn-on voltage of light. [c] Measured at 100 mA/cm^2. [d] Undetectable (less than 100 mA/cm^2).

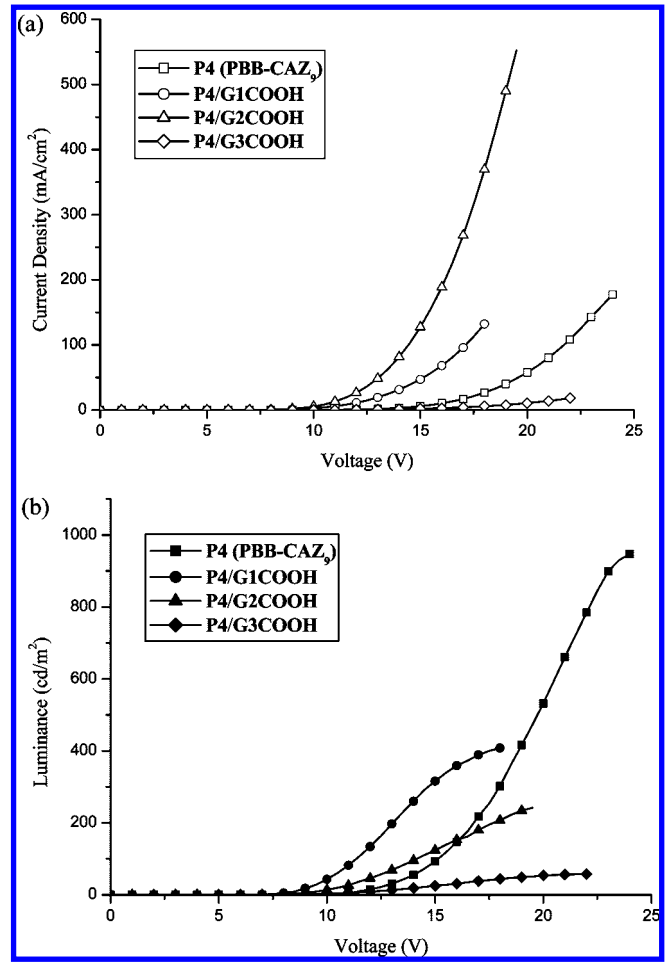

Figure 11. (a) Current density−voltage ($I-V$) curves and (b) luminance−voltage ($L-V$) curves of PLED devices with the configuration of ITO/PEDOT:PSS/polymer (**P4** or its H-bonded side-chain dendritic complexes)/BCP/Alq_3/LiF/Al.

0.39 cd/A at 100 mA/cm^2, respectively, which are generally better than those of corresponding PLED devices bearing H-bonded dendritic complexes **P4/G2COOH** and **P4/G3COOH**. This could be presumably attributed to the larger dendron shells of the higher generations of **OXD** H-donors, which have a larger influence on the carrier mobility and trapping process.[28,54]

Conclusion

A series of novel H-bonded acceptor copolymers containing different molar ratios of hole-transporting carbazole (**CAZ**) units and light-emitting **PBB** moieties (bearing three conjugated aromatic rings and a terminal H-acceptor) were successfully synthesized. By the complementary surroundings via the complexation with different generations of **OXD** dendritic donors (**G1COOH**−**G3COOH**), the emission wavelengths of H-acceptor copolymers can be easily adjusted in their self-assembled structures of H-bonded side-chain dendritic complexes. As a result, all light-emitting, hole-transporting, and charge-transporting groups possessing novel photophysical and thermal properties are obtained in the supramolecular side-chain copolymers (i.e., H-bonded side-chain dendritic complexes). Moreover, the incorporation of carbazole units in the acceptor copolymers shows higher glass transition temperatures than the acceptor homopolymer itself, and the emission wavelengths of H-acceptor polymers can be tuned (up to 61 nm of red shift) by H-bonds. In addition, the larger dendritic size (i.e., the higher generation) of H-donors can afford stronger site-isolation and dendron-dilution effects, and thus better energy-transfer phenomena can be achieved. The PLED devices with the configuration of ITO/PEDOT:PSS/(**P4** or its H-bonded dendritic complexes)/BCP/Alq_3/LiF/Al were fabricated, and the emission colors from blue to green can be effectively tuned by incorporating various generations of **OXD** dendritic donors in the supramolecular side-chain polymer structures.

Acknowledgment. We are grateful to the National Center for High-performance Computing for computer time and facilities. The powder XRD measurements are supported by beamline BL17A (charged by Dr. Jey-Jau Lee) of the National Synchrotron Radiation Research Center (NSRRC), in Taiwan. Prof. Yu-Tai Tao (vacuum deposition) at Institute of Chemistry, Academia Sinica (in Taiwan), is also acknowledged for his instrumental support in the PLED device fabrication. The financial support provided by the National Science Council of Taiwan (ROC) through NSC 95-2113-M-009-023 and Chung-Shan Institute of Science and Technology (in Taiwan) is acknowledged for this project.

Supporting Information Available: Experimental details of the XRD installation; ^{1}H NMR spectra and TGA data of monomers **M1**−**M2** and polymers **P1**−**P6**; XRD and POM data of homopolymer **P1**; chemical structure of model compound **1** and its emission spectrum overlapped with that of homopolymer **P5** as well as overlapped with the absorption spectrum of homopolymer **P1**. This material is available free of charge via the Internet at http://pubs.acs.org.

References and Notes

(1) Lehn, J. M. *Supramolecular Chemistry; Concepts and Perspectives*; VCH: Weinheim, Germany, 1995.
(2) (a) Jenekhe, S. A.; Chen, X. L. *Science* **1999**, *283*, 372. (b) Whiteside, G. M.; Mathias, J. P.; Seto, C. T. *Science* **1991**, *254*, 1312.
(3) Kato, T.; Fréchet, J. M. J. *Macromolecules* **1989**, *22*, 3819.
(4) Kato, T.; Kihara, H.; Kumar, U.; Uryu, T.; Fréchet, J. M. J. *Angew. Chem., Int. Ed. Engl.* **1994**, *33*, 1644.
(5) Malik, S.; Dhal, P. K.; Mashelkar, R. A. *Macromolecules* **1995**, *28*, 2159.
(6) Kato, T.; Kihara, H.; Ujiie, S.; Uryu, T.; Fréchet, J. M. *J. Macromolecules* **1996**, *29*, 8734.
(7) (a) Schenning, A. P. H. J.; Jonkheijm, P.; Peeters, E.; Meijer, E. W. *J. Am. Chem. Soc.* **2001**, *123*, 409. (b) Ligthart, G. B. W. L.; Ohkawa, H.; Sijbesma, R. P.; Meijer, E. W. *J. Am. Chem. Soc.* **2005**, *127*, 810. (c) Roosma, J.; Mes, T.; Leclère, P.; Palmans, A. R. A.; Meijer, E. W. *J. Am. Chem. Soc.* **2008**, *130*, 1120.
(8) Medvedev, A. V.; Barmatov, E. B.; Medvedev, A. S.; Shibaev, V. P.; Ivanov, S. A.; Kozlovsky, M.; Stumpe, J. *Macromolecules* **2005**, *38*, 2223.
(9) (a) Cheng, Z.; Ren, B.; Shan, H.; Liu, X.; Tong, Z. *Macromolecules* **2008**, *41*, 2656.
(10) Canilho, N.; Kasëmi, E.; Schlüter, A. D.; Mezzenga, R. *Macromolecules* **2007**, *40*, 2822.
(11) Dinolfo, P. H.; Hupp, J. T. *Chem. Mater.* **2001**, *13*, 3113.
(12) McClenaghan, N. D.; Passalacqua, R.; Loiseau, F.; Campagna, S.; Verheyde, B.; Hameurlaine, A.; Dehaen, W. *J. Am. Chem. Soc.* **2003**, *125*, 5356.
(13) Chen, Y. Y.; Tao, Y. T.; Lin, H. C. *Macromolecules* **2006**, *39*, 8559.
(14) Kimura, M.; Sano, M.; Muto, T.; Hanabusa, K.; Shirai, H. *Macromolecules* **1999**, *32*, 7951.
(15) Frein, S.; Auzias, M.; Sondenecker, A.; Vieille-Petit, L.; Guintchin, B.; Maringa, N.; Süss-Fink, G.; Barberá, J.; Deschenaux, R. *Chem. Mater.* **2008**, *20*, 1340.
(16) Burroughes, J. H.; Bradley, D. D. C.; Brown, A. R.; Marks, R. N.; Mackay, K.; Friend, R. H.; Burn, P. L.; Holmes, A. B. *Nature (London)* **1990**, *347*, 539.
(17) Mitschke, U.; Bäuerle, P. *J. Mater. Chem.* **2001**, *10*, 1471.
(18) Kawamoto, M.; Mochizuki, H.; Ikeda, T.; Iino, H.; Hanna, J. I. *J. Phys. Chem. B* **2005**, *109*, 9226.
(19) Johansson, D. M.; Srdanov, G.; Yu, G.; Theander, M.; Inganas, O.; Anderson, M. R. *Macromolecules* **2000**, *33*, 2525.
(20) Zaumseil, J.; Sirringhaus, H. *Chem. Rev.* **2007**, *107*, 1296.
(21) (a) Greenham, N. C.; Moratti, S. C.; Bradley, D. D. C.; Friend, R. H.; Holmes, A. B. *Nature (London)* **1993**, *365*, 628. (b) Burn, P. L.; Kraft, A.; Baigent, D. R.; Bradley, D. D. C.; Brown, A. R.; Friend, R. H.; Gymer, R. W.; Holmes, A. B.; Jackson, R. W. *J. Am. Chem. Soc.* **1993**, *115*, 10117.
(22) Marsitzky, D.; Vestberg, R.; Blainey, P.; Tang, B. T.; Hawker, C. J.; Carter, K. R. *J. Am. Chem. Soc.* **2001**, *123*, 6965.
(23) (a) Setayesh, S.; Grimsdale, A. C.; Weil, T.; Enkelmann, V.; Müllen, K.; Meghdadi, F.; List, E. J. W.; Leising, G. *J. Am. Chem. Soc.* **2001**, *123*, 946. (b) Pogantsch, A.; Wenzl, F. P.; List, E. J. W.; Leising, G.; Grimsdale, A. C.; Müllen, K. *Adv. Mater.* **2002**, *14*, 1061. (c) Oesterling, I.; Müllen, K. *J. Am. Chem. Soc.* **2007**, *129*, 4595.
(24) Kwok, C. C.; Wong, M. S. *Chem. Mater.* **2002**, *14*, 3158.
(25) Kimoto, A.; Masachika, K.; Cho, J. S.; Higuchi, M.; Yamamoto, K. *Chem. Mater.* **2004**, *16*, 5706.
(26) Pillow, J. N. G.; Halim, M.; Lupton, J. M.; Burn, P. L.; Samuel, I. D. W. *Macromolecules* **1999**, *32*, 5985.
(27) Kwon, T. W.; Alam, M. M.; Jenekhe, S. A. *Chem. Mater.* **2004**, *16*, 4657.
(28) (a) Kimura, M.; Sato, M.; Adachi, N.; Fukawa, T.; Kanbe, E.; Shirai, H. *Chem. Mater.* **2007**, *19*, 2809.
(29) Ma, C.-Q.; Mena-Osteritz, E.; Debaerdemaeker, T.; Wienk, M. M.; Janssen, R. A. J.; Bauerle, P. *Angew. Chem., Int. Ed.* **2007**, *46*, 1679.
(30) Taranekar, P.; Fulghum, T.; Patton, D.; Ponnapati, R.; Clyde, G.; Advincula, R. *J. Am. Chem. Soc.* **2007**, *129*, 12548.
(31) Burm, P. L.; Lo, S. C.; Samuel, I. D. W. *Adv. Mater.* **2007**, *19*, 1675.
(32) (a) Precup-Blaga, F. S.; Garcia-Martinez, J. C.; Schenning, A. P. H. J.; Meijer, E. W. *J. Am. Chem. Soc.* **2003**, *125*, 12953. (b) Schenning, A. P. H. J.; Peeters, E.; Meijer, E. W. *J. Am. Chem. Soc.* **2000**, *122*, 4489.
(33) Zhao, Z.; Xu, X.; Wang, H.; Lu, P.; Yu, G.; Liu, Y. *J. Org. Chem.* **2008**, *73*, 594.
(34) (a) Bo, Z.; Zhang, C.; Severin, N.; Rabe, J. P.; Schlüter, A. D. *Macromolecules* **2000**, *33*, 28–2688. (b) Fu, Y.; Li, Y.; Li, J.; Yan, S.; Bo, Z. *Macromolecules* **2004**, *37*, 6395. (c) Zhu, B.; Han, Y.; Sun, M.; Bo, Z. *Macromolecules* **2007**, *40*, 4494.
(35) Lo, S. C.; Burn, P. L. *Chem. Rev.* **2007**, *107*, 1097.
(36) Köse, M. E.; Mitchell, W. J.; Kopidakis, N.; Chang, C. H.; Shaheen, S. E.; Kim, K.; Rumbles, G. *J. Am. Chem. Soc.* **2007**, *129*, 14257.
(37) Wu, C. W.; Lin, H. C. *Macromolecules* **2006**, *39*, 7985.
(38) Eaton, D. *Pure Appl. Chem.* **1998**, *60*, 1107.
(39) Lin, D. G.; Lin, G. Q. *Tetrahedron Lett.* **1999**, *40*, 337.
(40) (a) Okawara, R.; Wada, M. *J. Organomet. Chem.* **1963**, *1*, 81. (b) Wada, M.; Nishino, M.; Okawara, R. *J. Organomet. Chem.* **1965**, *3*, 70.
(41) Engels, C.; Steenwinckel, D. V.; Hendrickx, E.; Schaerlaekens, M.; Persoons, A.; Samyn, C. *J. Mater. Chem.* **2002**, *12*, 951.
(42) Hathaway, B. A.; Taylor, B. E.; Wittenborn, J. S. *Synth. Commun.* **1998**, *28*, 4629.
(43) (a) Arbuzov, B. A. *Pure Appl. Chem.* **1964**, *9*, 307. (b) Michaelis, A.; Kaehne, R. *Chem. Ber.* **1898**, *31*, 1048.

(44) (a) Horner, L. *Chem. Ber.* **1958**, *83*, 733. (b) Wadsworth, W. S.; Emmons, W. D. *J. Am. Chem. Soc.* **1961**, *83*, 1733.
(45) Sonogashira, K.; Tohda, Y.; Hagihara, N. *Tetrahedron Lett.* **1975**, 4467.
(46) Cui, L.; Lattermann, G. *Macromol. Chem. Phys.* **2002**, *203*, 2432.
(47) Lin, H. C.; Hendrianto, J. *Polymer* **2005**, *46*, 12146.
(48) (a) Kumar, U.; Kato, T.; Fréchet, J. M. J. *J. Am. Chem. Soc.* **1992**, *114*, 6630. (b) Kato, T.; Fréchet, J. M. J.; Wilson, P. G.; Saito, T.; Uryu, T.; Fujishima, A.; Jin, C.; Kaneuchi, F. *Chem. Mater.* **1993**, *5*, 1094. (c) Kato, T.; Kihara, H.; Uryu, T.; Fujishima, A.; Fréchet, J. M. J. *Macromolecules* **1992**, *25*, 6836.
(49) (a) Kong, X.; Tang, B. Z. *Chem. Mater.* **1998**, *10*, 3352. (b) Lam, J. W. Y.; Dong, Y.; Law, C. C. W.; Dong, Y.; Cheuk, K. K. L.; Lai, L. M.; Li, Z.; Sun, J.; Chen, H.; Zheng, Q.; Kwok, H. S.; Wang, M.; Feng, X.; Shen, J.; Tang, B. Z. *Macromolecules* **2005**, *38*, 3290.
(50) (a) Wu, C. W.; Tsai, C. M.; Lin, H. C. *Macromolecules* **2006**, *39*, 4298. (b) Wu, C. W.; Sung, H. H.; Lin, H. C. *J. Polym. Sci., Part A: Polym. Chem.* **2006**, *44*, 6765.
(51) (a) Lin, H. C.; Sheu, H. Y.; Chang, C. L.; Tsai, C. *J. Mater. Chem.* **2001**, *11*, 2958.
(52) Leeuw, D. M.; Simenon, M. M. J.; Brown, A. R.; Einerhand, R. E. F. *Synth. Met.* **1997**, *87*, 53.
(53) Zhao, L.; Li, C.; Zhang, Y.; Zhu, X. H.; Peng, J.; Cao, Y. *Macromol. Rapid Commun.* **2006**, *27*, 914.
(54) Qu, J. Q.; Zhang, J. Y.; Grimsdale, A. C.; Müllen, K.; Jaiser, F.; Yang, X. H.; Neher, D. *Macromolecules* **2004**, *37*, 8297.

MA801005C